Space Weather

RESEARCH ARTICLE
10.1029/2025SW004610

Special Collection:
Space Weather Events of 2024 May 9-15

The New Geomagnetic Monitoring Network in China: Insights From the 2024 Mother's Day Superstorm

Jing Wang[1], Yue Yan[2], Bingxian Luo[1,3], Chunming Liu[2], Hui Li[1], Jiaojiao Zhang[1], Yanhong Chen[1], Chen Wu[2], Zihan Wu[2], Ziqian Liu[1], Xin Wang[1], Ercha Aa[1], and Xianzhi Ao[1]

[1]State Key Laboratory of Solar Activity and Space Weather, National Space Science Center, Chinese Academy of Sciences, Beijing, China, [2]North China Electric Power University, Beijing, China, [3]University of Chinese Academy of Sciences, Beijing, China

Key Points:

- The measured horizontal geomagnetic field disturbance of the May 2024 superstorm in China reaches −720 nT
- The impact of this superstorm on the Eastern Inner Mongolia Power Grid is comparable to that of the extreme geomagnetic storm in 1989
- A practical geomagnetically induced current (GIC) prediction model is proposed and evaluated by comparing the simulated GIC to the measurement

Correspondence to:
B. Luo and Y. Yan,
luobx@nssc.ac.cn;
yyue@ncepu.edu.cn

Citation:
Wang, J., Yan, Y., Luo, B., Liu, C., Li, H., Zhang, J., et al. (2026). The New geomagnetic monitoring network in China: Insights from the 2024 Mother's Day superstorm. *Space Weather*, *24*, e2025SW004610. https://doi.org/10.1029/2025SW004610

Received 7 JUL 2025
Accepted 2 FEB 2026

Author Contributions:
Conceptualization: Yue Yan, Bingxian Luo
Data curation: Jing Wang, Yue Yan, Hui Li, Chen Wu, Zihan Wu, Ziqian Liu
Formal analysis: Jing Wang, Yue Yan, Hui Li
Funding acquisition: Bingxian Luo, Chunming Liu, Hui Li
Methodology: Jing Wang, Yue Yan, Bingxian Luo, Chunming Liu, Jiaojiao Zhang
Project administration: Bingxian Luo, Chunming Liu
Supervision: Bingxian Luo, Chunming Liu, Jiaojiao Zhang, Yanhong Chen

Abstract China has established a ground-based network system, that is the Chinese Meridian Project (CMP), to continuously monitor the geomagnetic field. The superstorm in May 2024 was analyzed using the CMP data. The negative peak of the horizontal geomagnetic field (B_h) during the storm main phase at different CMP stations varied between −449 nT and −720 nT while the absolute peak value of the corresponding time derivative (dB_h/dt) varied from 32 nT/min to 60 nT/min. We adopted a geomagnetically induced current (GIC) model to investigate the impact of the storm on the Eastern Inner Mongolia Power Grid. The comparison between modeled and measured geomagnetically induced currents (GICs) at two substations showed a good agreement in timing and amplitude. The simulated GICs across the Eastern Inner Mongolia Power Grid service area identified the Tianjin South substation at 1,000 kV level as the most vulnerable part of the grid, with maximum GIC of 168.5 A. The GIC level, as an indicator, supports the conclusion that the effect of the May 2024 storm exceeds that of the November 2004 storm and is on a par with the March 1989 geomagnetic storm. Together with real-time GIC monitoring, our approach has paved the way for future geomagnetic storm risk assessment and extreme space weather safeguard.

Plain Language Summary The transient solar wind can disturb the Earth's magnetic field, forming a space weather phenomenon called geomagnetic storm. Large geomagnetically induced currents can damage the transformers and even cause a power grid blackout. The superstorm that occurred from May 10 to 12, 2024 set a new record of geomagnetic disturbance over the past two decades. How strong was the geomagnetic disturbance over China and how did the power grid respond to the extreme geomagnetic storm? We try to answer these questions in this paper with the help of domestic data coming from both the geomagnetic stations and the power grid.

1. Introduction

To improve our understanding of the solar-terrestrial physical processes, a large-scale ground-based space environmental monitoring network, that is the Chinese Meridian Project (CMP), has been completed in China (Wang, 2010; Wang et al., 2024). The CMP consists of nearly 300 instruments distributed at 31 stations. The stations are tactically positioned along 120°E and 100°E in longitude and 30°N and 40°N in latitude, with the observation covering the entire causal chain from the Sun to the Earth. The Geomagnetic Monitoring Network Subsystem of the CMP has deployed 109 geomagnetic instruments to measure the geomagnetic field fluctuations of various time scales.

One of the major space weather effects on the Earth is the so-called geomagnetic storm. Intense geomagnetic storms may spark power grid blackout, damage satellites, and disrupt communication and navigation systems. During such storms geomagnetically induced currents (GICs) are generated in ground conductive infrastructure including power grids, pipelines and railways, to name a few (Boteler & Pirjola, 2017; Liu et al., 2016). Large GIC in transformer's windings can saturate its core, causing a malfunction or permanent damage. The worst-case scenario is a system-wide failure (Pirjola, 2002). The corresponding increase of the pipe-soil potentials offset can disrupt cathodic protection systems, and hence accelerates the pipeline corrosion (Boteler, 2000). Since the GICs during major geomagnetic storms have the potential to disrupt high-voltage power transmission systems wide-spread, the interest from policymakers, scientists, industry leaders, and the public is increasing (Pulkkinen et al., 2017). The most serious power grid catastrophe well known to the space weather community was the

Writing – original draft: Jing Wang, Yue Yan, Yanhong Chen
Writing – review & editing: Jing Wang, Yue Yan, Xin Wang, Ercha Aa, Xianzhi Ao

Hydro-Québec power outage during the March 1989 geomagnetic storm. Geomagnetically induced current was believed to be the main culprit. Millions of Hydro-Québec customers experienced a nine-hour power outage during the cold winter. The GICs also damaged several extra-high-voltage transformers in the US (Jonas & McCarron, 2015).

A very intense geomagnetic storm occurred on 10–12 May 2024, driven by multiple Coronal Mass Ejections (CMEs) that erupted between May 7 and 9. The geomagnetic Kp index reached the top level of 9. The geomagnetic disturbance storm time (Dst) index dropped to a minimum of −412 nT on May 11, making it the most intense geomagnetic storm in the past two decades. The storm, also known as the Mother's Day storm or the Gannon storm, sparked worldwide interest in the space weather community (Hayakawa et al., 2024; Caraballo et al., 2025; Spogli et al., 2024; Kwak et al., 2024; Waghule & Knipp, 2024; Wang et al., 2025; Aa et al., 2024; Chen et al., 2025). Adopting a ground electric field model based on magnetotelluric data, Lawrence et al. (2025) utilized the geomagnetic station data, and the high-voltage power grid network information to estimate the GICs at substation level during the storm in the UK. The highest modeled GICs exceeded 60 A in substations in southwest and east–central England as well as northern Wales. Additionally, Piersanti and Oliveira. (2025) investigated the effect of geomagnetically induced electric fields (GIEs), and hence GICs, during the sudden storm commencement (SSC) on 10 May 2024 over Europe, using the European quasi-Meridional Magnetometer Array. However, the effect of this geomagnetic storm, particularly GICs, at middle latitudes over the East Asian sector, remains unknown.

We present our analysis of the geomagnetic disturbance over China and the effect of the GICs on the Eastern Inner Mongolia Power Grid in China for the very intense Mother's Day storm. The data are from the geomagnetic stations supported by the CMP. The amplitude and vector variation of the H component and the time derivative of the geomagnetic perturbations (dB_h/dt, dB_x/dt, dB_y/dt) are discussed. The impact of the storm on the Eastern Inner Mongolia Power Grid is assessed by the GIC level, which is compared to those of the March 1989 and November 2004 storms.

The paper is arranged as follows. In Section 2, we explain the data and our modeling process. Subsection 3.1 presents a detailed description of the local geomagnetic disturbances using the available CMP measurements. Subsection 3.2 shows the GICs response to the storm and its impact on the Eastern Inner Mongolia Power Grid. Subsection 3.3 compares the impacts to those of the storms in 2004 and 1989. Section 4 discusses the impact of this geomagnetic storm on power grids in other mid-to low-latitude countries and the implication of this event for improving geomagnetic storm preparedness and mitigation strategies in the Eastern Inner Mongolia Power Grid. We summarize our results and findings in Section 5.

2. Data and Methodology

2.1. The Extraction of Geomagnetic Disturbance

The CMP geomagnetic monitoring stations are equipped with the fluxgate theodolite, the Overhauser magnetometer and fluxgate magnetometers. The fluxgate theodolite measures the baseline values of the geomagnetic field, the Overhauser magnetometer measures the total geomagnetic field intensity, and the fluxgate magnetometer measures the relative variations of the H, D, Z components of the geomagnetic field in 1-s cadence. The geomagnetic data used in this study are the external variations only. In order to extract the external field data, we selected five International Quiet Days (IQDs) in April 2024 issued by World Data Center for Geomagnetism, Kyoto (available at https://wdc.kugi.kyoto-u.ac.jp/), computed the average of each component over those days, and subtracted the respective averages from the measured data. All times reported in this study are in Universal Time (UT). Based on the assumption that the change in the D component is small, a corresponding angular change $\triangle D$ (in degrees) can be converted into the variation B_D (in nT):

$$B_D = \left(\triangle D \times \pi \times B_{HA}\right)/180 \quad (1)$$

Where $\triangle D$ represents the relative variation of the D component in degrees, B_D represents the relative variation of the D component in nT and B_{HA} denotes the annual average value of the H component at the local geomagnetic

Table 1
Chinese Meridian Project Geomagnetic Stations

Number	Code	Latitude	Longitude
1	OMOHE	53.49°N	122.34°E
2	OYAKS	50.48°N	121.69°E
3	OMZLN	49.57°N	117.45°E
4	OHUTB	44.36°N	86.94°E
5	ONOAN	44.09°N	124.91°E
6	OCSSL	40.30°N	116.19°E
7	OJIYG	39.81°N	98.22°E
8	ODLZS	39.58°N	121.77°E
9	OKSHI	39.51°N	75.81°E
10	OHBLF	39.50°N	116.70°E
11	OQIMO	38.14°N	85.45°E
12	OGERM	36.43°N	94.87°E
13	OTANC	34.70°N	118.46°E
14	OGAER	32.52°N	80.11°E
15	OYICH	30.92°N	113.34°E
16	OPIXI	30.91°N	103.76°E
17	OHZXH	30.25°N	120.11°E
18	OLSCG	29.63°N	91.04°E
19	OLJGC	26.97°N	100.18°E
20	ONANA	25.02°N	118.51°E
21	OZHQI	23.05°N	113.20°E
22	OQIZH	19.03°N	109.85°E
23	OLEDO	18.44°N	108.97°E

station. The 23 operational stations of the CMP Geomagnetic Observatory Network span nearly the entire mainland China, covering longitudes approximately from 75°E to 122°E and latitudes from 18°N to 54°N. Our research focuses on the geomagnetic and GICs response during the geomagnetic storms from low-latitude to mid-latitude regions over China with the help of the CMP data. The station code, latitude, and longitude are shown in Table 1. Figure 1 is the schematic of the station locations and the Eastern Inner Mongolia Power Grid service area.

The sampling rate of the data is 1 s. The unreliable data were removed and then the 1-s data were converted into 1-min resolution utilizing a Gaussian filter for further analysis. In order to extract the geomagnetic disturbance, we selected five IQDs in April issued by the World Data Center for Geomagnetism, Kyoto (WDC-Kyoto, available at https://wdc.kugi.kyoto-u.ac.jp/).

To calculate the vector variation of $\vec{H}$, we adopted an approximate method, that is simply let B_D and B_h represent the eastward and northward variations of respectively in the local Cartesian coordinate system with the station location as the origin.

The time derivative of the geomagnetic field perturbations dB_h/dt can be obtained from Equation 2.

$$dB_h/dt = (B_h(t_2) - B_h(t_1))/(t_2 - t_1) \quad (2)$$

where $B_h(t_1)$ and $B_h(t_2)$ represent the measured horizontal component intensity of the magnetic field at times t_1 and t_2 respectively, $(t_2 - t_1)$ denotes the time interval between the two measurements, which is set to 1 min.

2.2. GIC Modeling in the Eastern Inner Mongolia Power Grid

The Eastern Inner Mongolia Power Grid, managed by State Grid Inner Mongolia Eastern Electric Power, approximately covers a range of 41°N ~ 53°N in latitude and 116°E ~ 126°E in longitude. The monitoring data at the OMZLN, OMOHE, ONOAN, and OCSSL geomagnetic stations were downloaded from the CMP data center for the period of May 10–12. These data were spatially interpolated using the Spherical Elementary Current Systems (SECS) method (Amm, 1997). This approach infers the equivalent ionospheric currents from ground-based geomagnetic field measurements and thereby estimates the geomagnetic field at substations from the geomagnetic stations.

Although the actual distribution of Earth's resistivity is highly complex, it is widely acknowledged that the most significant variations occur with depth rather than laterally at the surface. Consequently, the magnetotelluric (MT) sounding method is commonly employed to measure the Earth's conductivity profile. Jilin University carried out MT surveys in the Songliao Plain in Northeast China (Liu et al., 2008). Data were acquired using the MMS 02 MT sounding system manufactured by Metronix GmbH, with magnetic cassette tape recording. The frequency range was from 0.5 to 0.00033 Hz. A total of 15 high-frequency segments and 8 low-frequency segments were selected. Several MT profiles were obtained as shown in Figure 2. The MT survey area is co-located with the region monitored by the OMZLN, OMOHE, ONOAN and OCSSL geomagnetic stations, and lies entirely within the footprint of the Eastern Inner Mongolia Power Grid. The resulting geoelectrical parameters are considered representative and applicable for calculating the regional geoelectric field. Based on the resistivity data for the selected profiles (Liu et al., 2008), a one-dimensional conductivity model with vertical layering for the Eastern Inner Mongolia Power Grid was constructed, as presented in Table 2.

The geoelectric field is calculated using the plane wave theory (Cagniard, 1953), with the 1-D Earth conductivity model in the frequency domain (Viljanen et al., 2004), the x and y components of the induced geoelectric field $E_{x,y}$ can be calculated from the x and y components of geomagnetic perturbations $B_{y,x}$.

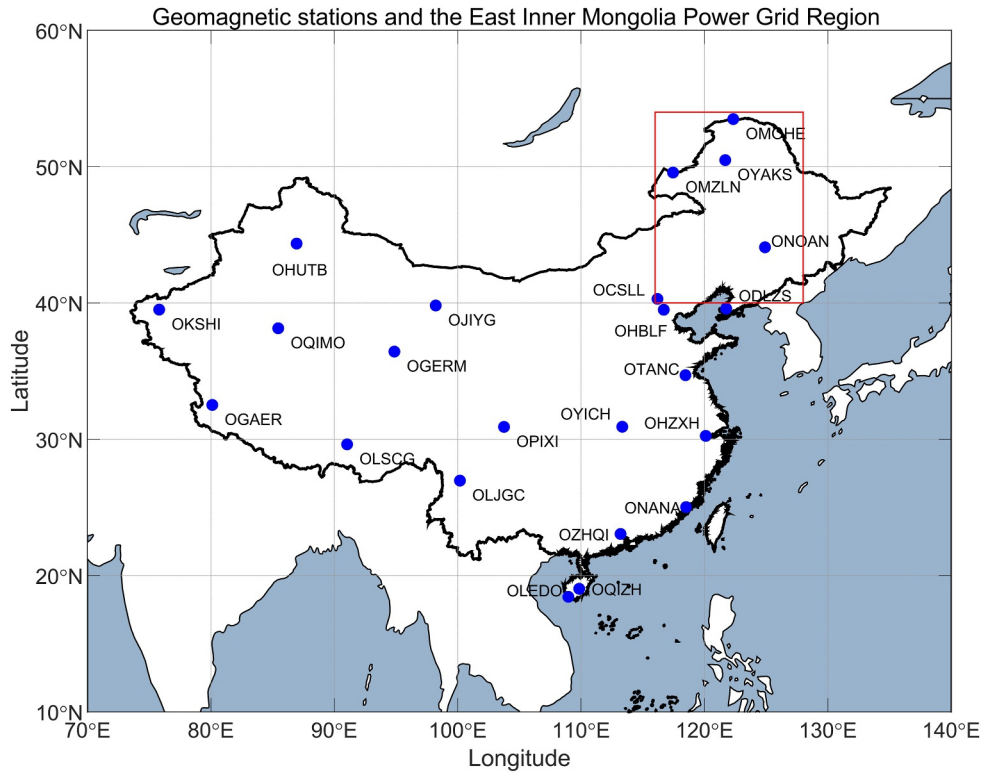

Figure 1. Schematic of the Chinese Meridian Project geomagnetic station locations. The solid blue circles represent the stations and the service area of the Eastern Inner Mongolia Power Grid is illustrated by the red square.

$$\dot{E}_x(w) = \frac{1}{\mu_0}\dot{B}_y(w)Z_0(w) \tag{3}$$

$$\dot{E}_y(w) = -\frac{1}{\mu_0}\dot{B}_x(w)Z_0(w) \tag{4}$$

where μ_0 is the vacuum permeability; the x and y subscripts denote the north and east geographic directions, respectively; the Earth's surface wave impedance Z_0 contains all the information about the Earth's electrical structure.

The nodal admittance matrix (NAM) method (Boteler, 2014) is applied to model the GICs in the Eastern Inner Mongolia Power Grid. The quasi-DC voltage generated by the induced geoelectric field between any two points on the ground within a power grid is calculated by performing a line integral of the electric field along the path connecting the two points:

$$V_{\mathrm{AB}} = \int_A^B \vec{E}\cdot\overrightarrow{\mathrm{dl}} \tag{5}$$

The equivalent current source in each line can be obtained through the voltage source. The sum of all equivalent current sources flowing into node k are expressed as the product of the node admittance matrix and the node voltage column vector

$$[J] = [Y][V]. \tag{6}$$

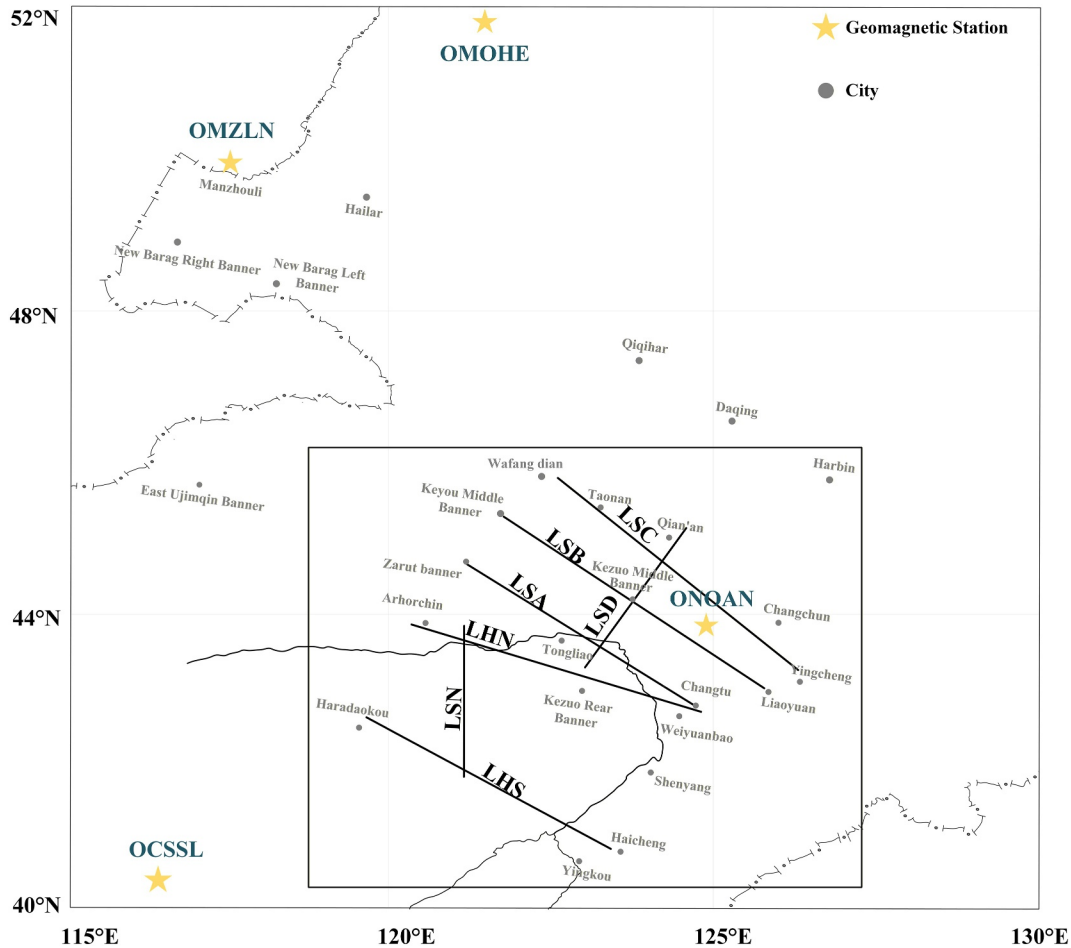

Figure 2. MT profiles in Songnan -northern Liaoning. The 7 black lines represent the 7 MT profiles. LSA: Zalut Banner - Changtu MT profile; LSB: Keyouzhongqi-Liaoyuan MT profile; LSC: Wafangdian-Yingchengzi MT profile; LSD: Kezuohouqi - Qianan MT profile; LSN: Beipiao-Xishaogen MT Profile; LHN: Aqi - Weiyuanbao MT profile; LHS: Haladaokou - Haicheng MT profile. The yellow stars denote the geomagnetic stations. The gray solid circles represent cities locations.

Table 2
One-Dimensional Vertically Layered Conductivity Model of the Eastern Inner Mongolia Power Grid

depth(km)	conductivity(S/m)	Layer thickness(km)
0–100	0.00067	100
100–150	0.001	50
150–200	0.00056	50
250–300	0.0004	50
>300	0.002	∞

$$Y_{kk} = y_k + \sum_{n=1}^{N} y_{nk} \quad k \neq i \tag{7}$$

$$Y_{nk} = -y_{nk} \tag{8}$$

Where the term y_k denotes the admittance to ground at node k and y_{nk} denotes the mutual admittance between nodes k and n. The diagonal element of the matrix, that is Y_{kk}, is the sum of the admittances of all branches connected to node k, while the off-diagonal element Y_{nk} is the negative of y_{nk}.

The Eastern Inner Mongolia Power Grid comprises of three voltage levels: 220 kV, 500 kV, and 1,000 kV. Based on the explanation given by "GIC-Benchmark" (Horton et al., 2015), a full-node model is employed to construct the GIC equivalent model for the multi-voltage-level power grid. The core challenge in modeling GIC in such systems lies in selecting valid nodes and branches to build the NAM. The busbars and neutral points of substations are treated as nodes in a quasi-DC circuit. The equivalent circuit includes transmission lines between busbars of the same voltage level and transformer

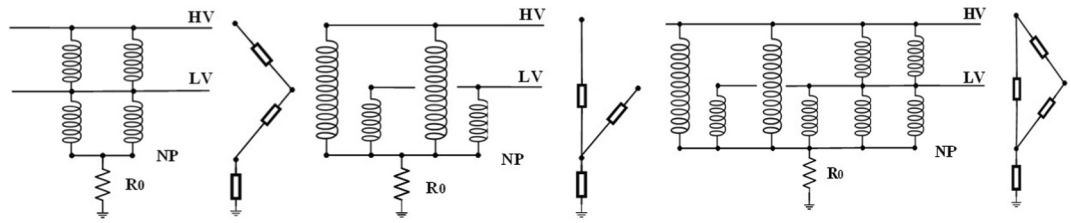

Figure 3. DC equivalent circuit for conventional transformers, autotransformers and hybrid configurations combining both conventional transformers and autotransformers.

winding branches connecting busbars of different voltage levels or linking busbars to neutral points.

Transformers provide the pathways for GIC to propagate between different voltage levels. The corresponding equivalent circuit depends on both the transformer winding configuration and the type of transformer. The transformers in the Eastern Inner Mongolia Power Grid adopt *Y* or *D* winding connection. In the Y-connected transformers, both the busbar and the neutral point are modeled as independent nodes, with the branch types defined based on the voltage levels of the terminals. In the D-connected transformers, zero-sequence currents form closed internal loops, where GICs, due to their quasi-DC nature, do not form a conductive path. Thus, the nodes and branches associated with D-connected transformers are excluded from the DC model of the network. In the full-node model, the high-voltage (HV) busbars, low-voltage (LV) busbars, and neutral points (NP) are represented as independent nodes. There are different types of transformers and combinations: (a) for a conventional transformer, the GIC equivalent circuit consists of HV–NP, LV–NP, and NP–ground branches; (b) for an autotransformer, the circuit includes HV–LV, LV–NP, and NP–ground branches; and (c) for a hybrid configuration combining both conventional transformers and autotransformers, the circuit includes four branches: HV–LV, HV–NP, LV–NP, and NP–ground. The DC network model parameters for the power grid are listed in Figure 3.

Table 3 lists the structural parameters of the Eastern Inner Mongolia power grid at various voltage levels, including the winding resistance, grounding resistance, and the per-unit-length transmission line resistance based on the design values of typical transformers and lines of China.

3. Results

3.1. The Geomagnetic Disturbance Over China

The geomagnetic disturbances of the 23 CMP stations, representing the external variations with quiet-day baselines removed as described in Section 2.1, are shown in Figures 4 and 5. The CME arrived at the Earth on 10 May 2025 and compressed the magnetopause, yielding a rapid increase in the H component of the geomagnetic field. This process is often referred to as a SSC or a sudden impulse (SI) depending on whether or not followed by enhanced geomagnetic activities (Araki, 1994; Matsushita, 1962). Figure 4 illustrates the shock arrival and the corresponding SSC at 17:07 UT on 10 May recorded at the 23 CMP stations. Figure 5 illustrate the strongest ground response of $B_h = 188$ nT was observed at the OYAKS station located at the second-highest latitude. The lowest variation associated with the SSC ($B_h = 103$ nT) was recorded at the OLEDO station, which is at the lowest latitude. The variations of B_h associated with the SSC in the area of the East Inner Mongolia Power Grid were between 139 nT (ONANA) and 188 nT (OYAKS).

Table 3
Eastern Inner Mongolia Power Grid Structural Parameters

Voltage (kV)	Transformer type	Resistance W1(ohm)	Resistance W2(ohm)	Grounding resistance(ohm)	Line resistance (ohm/km)
220	GSU	0.451	—	0.3	0.0365
500	Auto	0.238	0.097	0.2	0.0185
	GY-GY	0.335	—		
1,000	GY-GY	0.324	—	0.125	0.00727

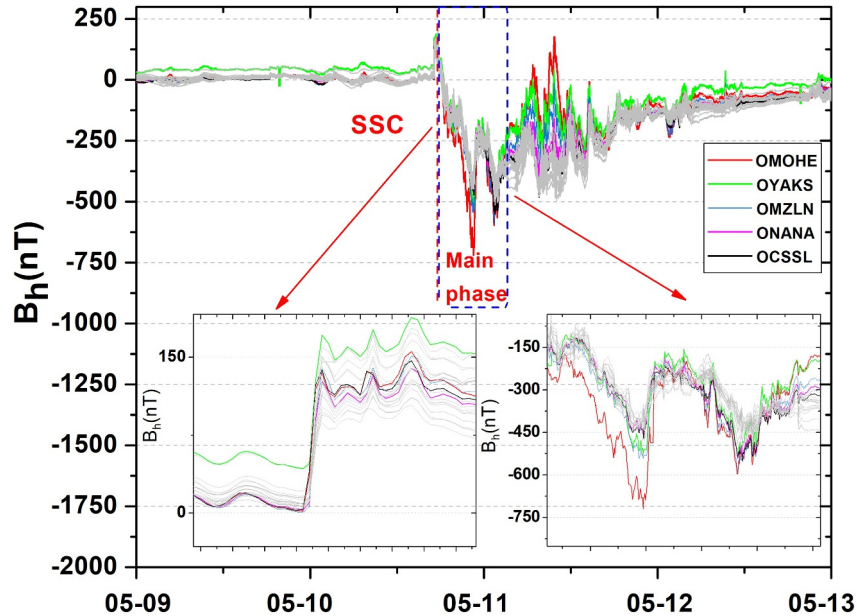

Figure 4. The amplitude variation of the H component (B_h) at the 23 Chinese Meridian Project stations during the storm. The left subplot shows a zoomed view of the sudden storm commencement, and the right subplot shows a zoomed view of the main phase. The colored lines represent the stations located near the East Inner Mongolia Power Grid while the gray lines represent the other stations.

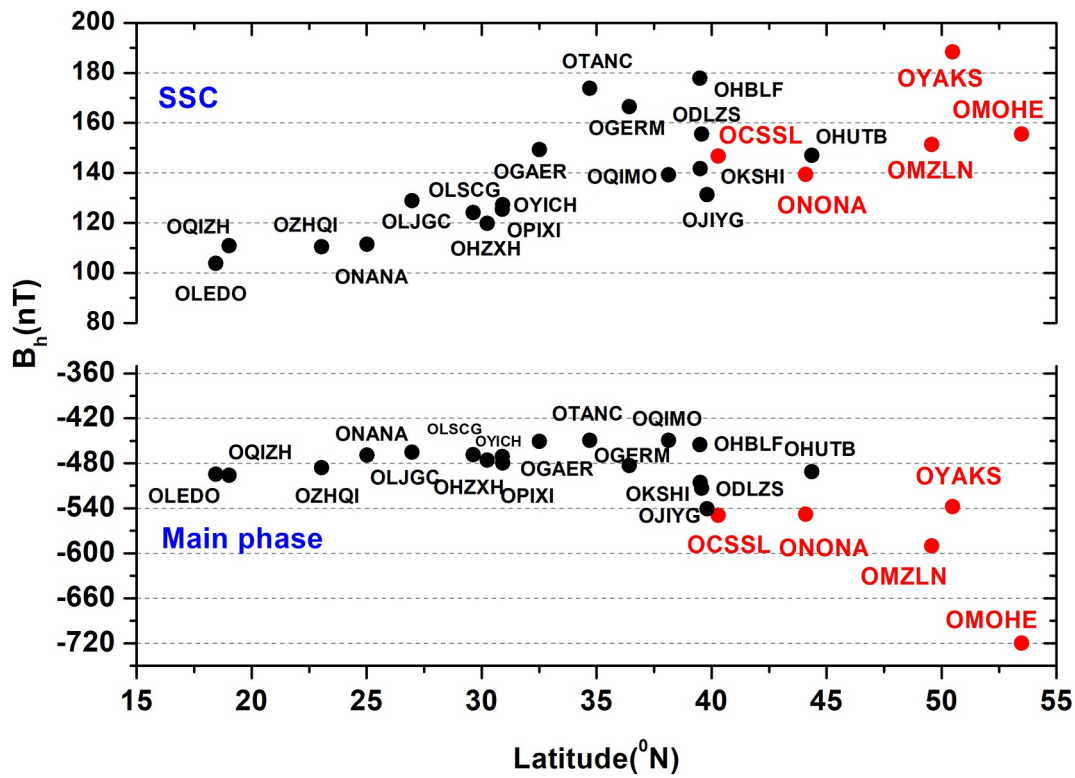

Figure 5. The maximum B_h during sudden storm commencement and the minimum B_h during the main phase of the geomagnetic storm. The red dots represent the stations located near the East Inner Mongolia Power Grid while the black dots represent the other stations.

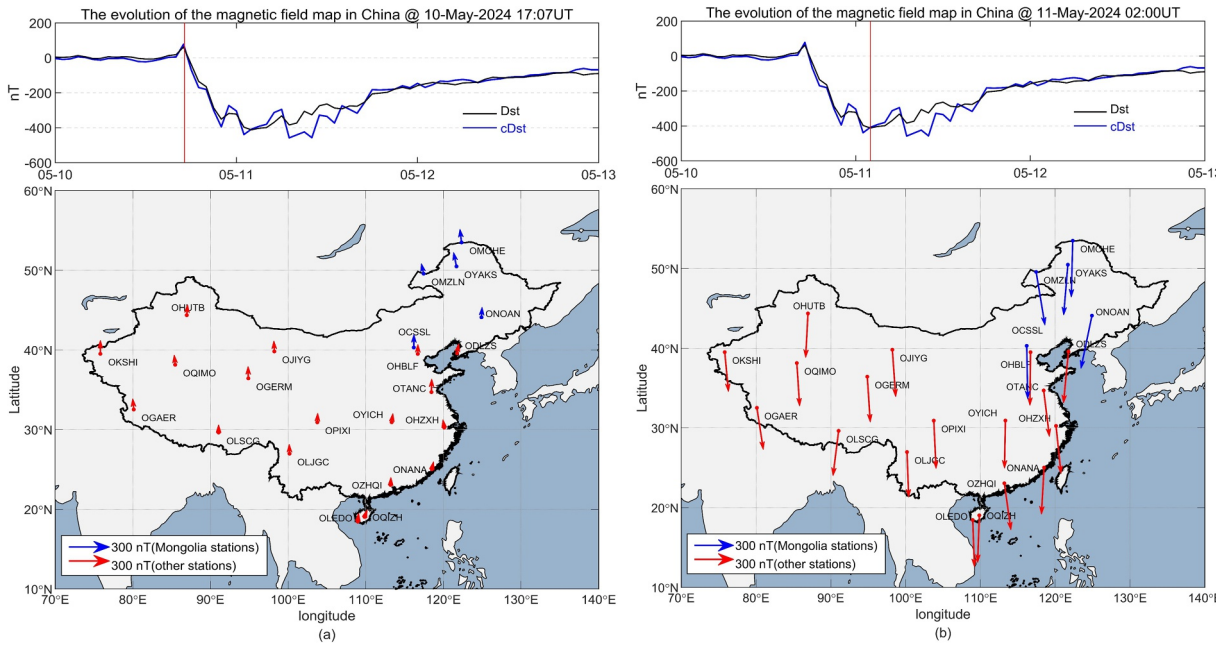

Figure 6. From left to right, the panels show the Dst, Cdst index and the vector variations of the H component during the sudden storm commencement (SSC) (a) and the main phase of the storm (b). The vertical red lines represent the start of SSC at 17:07 UT on 10 May (a) and the time of 02:00 UT on 11 May (b) when the Dst index reached the minimum of −412 nT, respectively. The blue arrows indicate the H-vector variations of stations located near the East Inner Mongolia Power Grid and the red arrows indicate the variations at other stations.

A sharp decrease in the H component is typically observed during the main phase of a geomagnetic storm, usually shortly after the SSC. In mainland China, the minimum B_h during the storm main phase varied between −449 nT (OTANC) and −720 nT (OMOHE). Since the Eastern Inner Mongolia Region is located at high latitude, it experiences relatively larger geomagnetic disturbance compared to other low latitude areas. The minimum B_h measured at stations covered by the East Inner Mongolia Power Grid varied between −538 nT (OYAKS) to −720 nT (OMOHE). The amplitude variation of the H component (B_h) at each individual station is presented in Appendix A.

Figure 6 presents the vector variation of the H component over China. At 17:07 UT on 10 May (Figure 6a), the vector H at the 23 stations showed upward trend due to the shock compression on the magnetopause which led to an abrupt increase of the H component in amplitude, that is the occurrence of the SSC. During the main phase of the storm, a number of charged particles from the magnetotail plasma sheet were injected into the ring current, which greatly enhanced the intensity of the southward magnetic field. When the Dst index reached the minimum of −412 nT and local Dst index (Cdst index, Li & Liu, 2023) reached the value of −408 nT at 02:00 UT on 11 May (Figure 6b), the H component experienced a sharp decrease, accompanied by downward change in its vector direction. This map illustrates the overall response of the CMP geomagnetic monitoring network to the storm. The animated evolution of the magnetic field map is presented in Appendix B with the form of GIF.

It is well-established that GICs are related to the time derivative of the geomagnetic field perturbations, that is dB_h/dt (Zhang et al., 2020, 2022). Figures 7 and 8 present the variations of dB_h/dt during the storm over China. Evidently, the amplitude variation of dB_h/dt is minimal during geomagnetic quiet time. By contrast, during the main phase of the storm the dB_h/dt varies more rapidly. As for the case discussed in this paper, the absolute peak value of dB_h/dt at the 23 stations varied between 32 nT/min and 60 nT/min with the largest values measured at the OMOHE station and smallest at the OQIZH station. Specifically, the dB_h/dt at the stations located in the Eastern Inner Mongolia Region exhibited greater fluctuations than the other stations being located at the higher latitude. The absolute peak value of dB_h/dt at these stations ranged between 42 nT/min and 60 nT/min. The amplitude variation of the dB_h/dt at each individual station is presented in Appendix A.

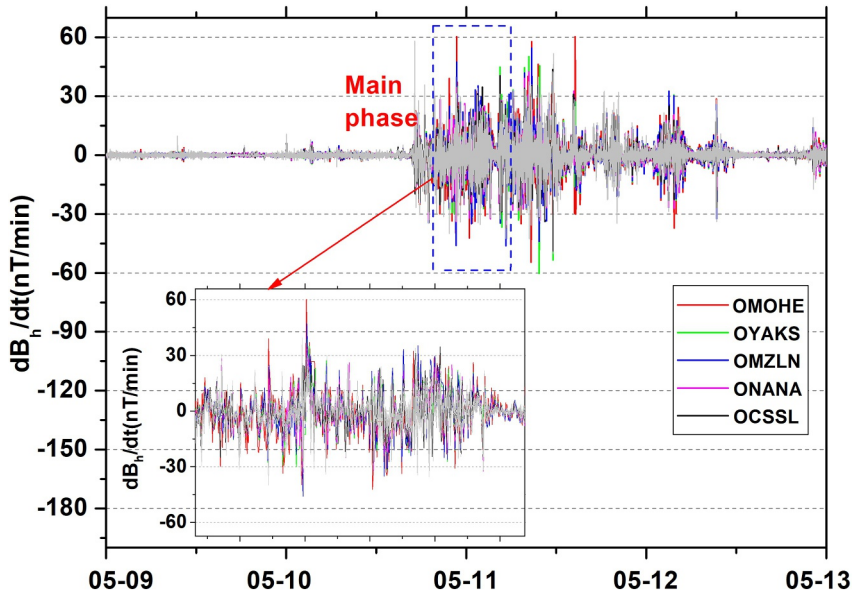

Figure 7. The time derivative of the horizontal component of the geomagnetic perturbations (dB_h/dt) from the 23 Chinese Meridian Project stations during May 9–12, 2024. The subplot shows the zoomed views during the main phase. The colored lines represent the stations located near the East Inner Mongolia Power Grid while the gray lines represent the other stations.

3.2. Impact on the Eastern Inner Mongolia Power Grid

As a grid at the terminal end of the Northeast China power grid, the Eastern Inner Mongolia power system has limited power supply capacity, and its complex hybrid AC/DC network configuration heightens the challenges to system stability, particularly during geomagnetic storms.

To monitor the operational status of the Eastern Inner Mongolia Power Grid, GIC monitoring devices have been installed at several substations. During the May 2024 super storm, the GIC monitoring devices installed at two

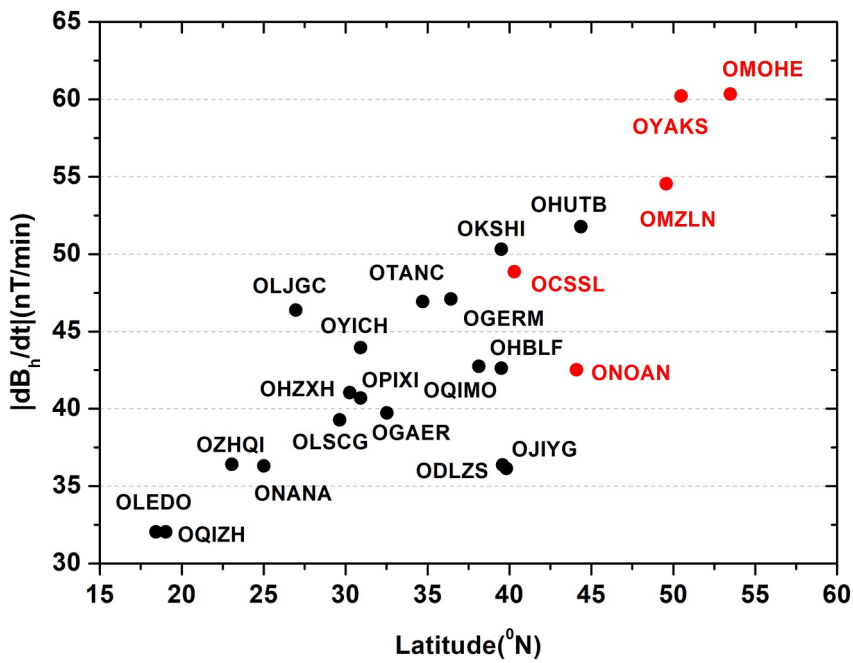

Figure 8. The absolute peak value of dB_h/dt during the main phase of the geomagnetic storm. The red dots represent the stations located near the East Inner Mongolia Power Grid while the black dots represent the other stations.

500 kV substations MCD and PIZ recorded valid GIC data between 07:00 UT and 11:30 UT on May 12 with a temporal resolution of 1 s. Prior to this interval, due to signal interruption or instrument failure, no GIC data was detected. After the interval, the recorded signals were flat and invalid for analysis.

Figure 11 illustrates that the MCD and PIZ substations serve as the two terminals for a southeast-trending 500 kV transmission line, and both act as major hubs where multiple power lines interconnect. The MCD Substation serves as an important corridor linking the Eastern Inner Mongolia energy base with the North and Northeast China power grids. It plays a key role in transmitting Mongolia's abundant wind and thermal power resources to major load centers in Liaoning, Jilin, and North China. The PIZ Substation is primarily responsible for collecting wind and solar power from the Xilingol League region. This energy is then transmitted via the ultra-high-voltage (UHV) lines to load centers in North and East China.

Unlike the conventional approach that monitors GICs through the transformer neutral point, the GIC monitoring systems at these two substations are installed directly on the conductors of the transformer's high-voltage input and output lines. These devices remain at the same electrical potential as the conductors and do not experience high voltage stress. The system collects the voltage signal from a single conductor and transmits the data wirelessly to a remote monitoring unit, where the GIC flowing through the transformer windings is computed. This configuration achieves the electrical isolation of the monitoring system from the high-voltage and high-current environment. The benefit is that it eliminates the risk of neutral-point overvoltage coupling into the substation's secondary system via power lines, which is commonly a concern with the neutral-point-based monitoring. It also resolves the issue that conventional low-voltage monitoring equipment often fails to meet required insulation standards, and hence enables a safe long-term online monitoring of the GIC in the power grid.

Figure 9 compares the simulated GICs to the measurements for the single-phase transformer winding at the two 500 kV substations. It is obvious that at both substations the time derivative of the geomagnetic field components (dB_x/dt, dB_y/dt) and the geoelectric field components (E_y, E_x) exhibited sudden variations at about 09:20(UT), coinciding with the GIC maximum. The next sharp variations in dB_x/dt, dB_y/dt, E_y, and E_x occurred at about 09:24(UT) due to the arrival of a shock (Hajra et al., 2024), when the GIC reached another extremum. At substation MCD, the simulated the simulated maximum absolute GIC value was 10.7 A while the measured absolute maximum value was 10.58 A, which yielded a relative error of 1.13%. At substation PIZ, the simulated maximum GIC was 12.3 A and the measured maximum GIC was 11.98 A, which yielded a relative error of 2.67%. The simulated GIC maximum amplitudes were slightly higher than the measured maximum values, which was primarily due to the neglect of the inductive effect in the GIC calculation process (Bolduc et al., 2000; Boteler & Bradley, 2016). The root mean square errors (RMSEs) of the simulations were 1.01 and 0.98 A for the two substations, respectively. Moreover, certain discrepancy between the simulation and measurement was observed at some time away from the peak. Since the GIC amplitudes during these intervals were relatively low, the electromagnetic noise arising from various uncertain factors became significant, and consequently led to a larger deviation at low GIC levels. The inaccuracies in both the characterization of the power grid's electrical structure and the Earth's conductivity profile also contributed to the discrepancies. Nevertheless, the influence of power grid topology on GICs is generally greater than that of the Earth's conductivity (Beggan, 2015).

Overall, the simulated GIC data show good agreement with the measurements in both the timing and the magnitude of the maximum values. During the storm period, a high correlation was observed between the interpolated dB_h/dt and the measured GICs at the two substations. Given the fact that the measured GIC data did not follow a normal distribution, Pearson correlation analysis was not applicable. Instead, the correlation was assessed using Spearman's rank correlation coefficient, yielding values of 0.78 and 0.83 for substations MCD and PIZ, respectively.

The good agreement between simulated and measured GICs at the two 500 kV substations validates our modeling approach for the Eastern Inner Mongolia Power Grid. The demonstrated accuracy in reproducing both the timing and magnitude of GIC peaks, with RMSE values of approximately 1 A, confirms that our methodology can be reliably applied to estimate GICs at other substations throughout the network where direct measurements are not available.

Since the 220 kV Manzhouli substation is located near the geomagnetic station of OMZLN, using the OMZLN data enables us to assess the geoelectric field and GICs at Manzhouli substation with a reasonable degree of accuracy during geomagnetic storms. The analysis for the May 10–12 event is presented in Figure 10. The SYM-H index, a high-resolution (1-min) geomagnetic activity indicator functionally equivalent to Dst but with superior

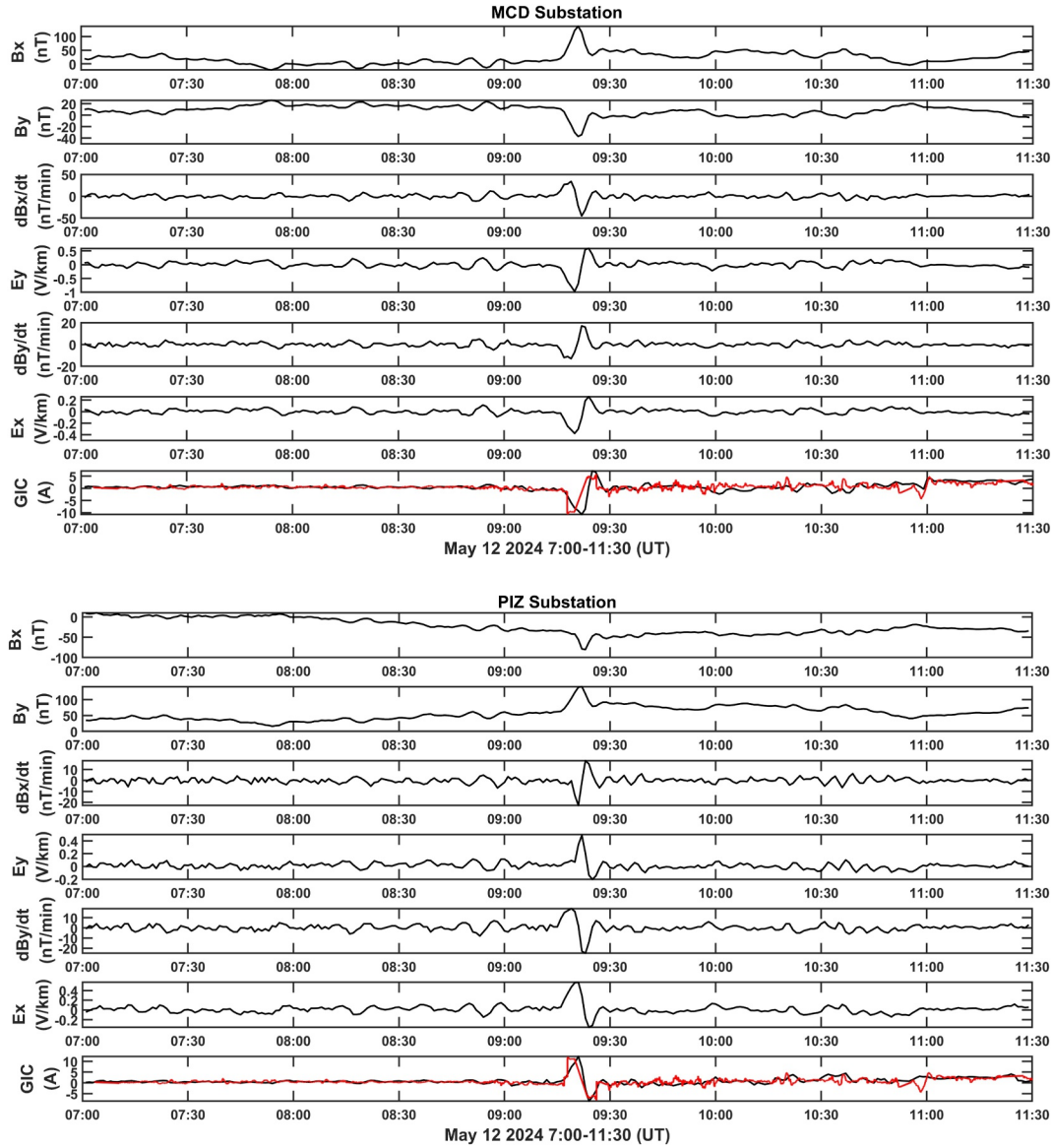

Figure 9. Comparison of the simulated geomagnetically induced currents to the observed data which flowed through the windings at two 500 kV substations on 12 May 2024. The black and red lines represent the calculated results and the observations, respectively.

temporal resolution, is used here instead of the hourly Dst to better resolve the rapid geomagnetic variations at Manzhouli substation. The 1-min cadence of SYM-H allows for more precise correlation with the sharp changes in dB_x/dt and dB_y/dt that drive the GIC variations shown in the bottom panels.

Significant variation in the induced geoelectric field was observed from the evening of May 10 through the afternoon of May 12, corresponding to the SSC, main phase and recovery phase. In general, the amplitude of the eastward electric field (E_y) was greater than that of the northward component (E_x). The maximum geoelectric field occurred during the SSC. A sharp increase in dB_x/dt was recorded at 17:07 UT on May 10, when Ey reached a negative peak of −1.67 V/km and the total geoelectric field magnitude reached the maximum of 1.68 V/km. Subsequently, the calculated GIC reached its maximum value of 20.1 A at 22:38 UT on May 10. The minor perturbation in SYM-H at 09:24 UT on May 12 corresponds to the shock arrival identified by Hajra (Hajra et al., 2024), which triggered the sharp geomagnetic changes and GIC response discussed previously for the MCD and PIZ substations. At this precise moment, E_y peaked at 0.79 V/km, while GIC attained a local maximum of 1.9 A.

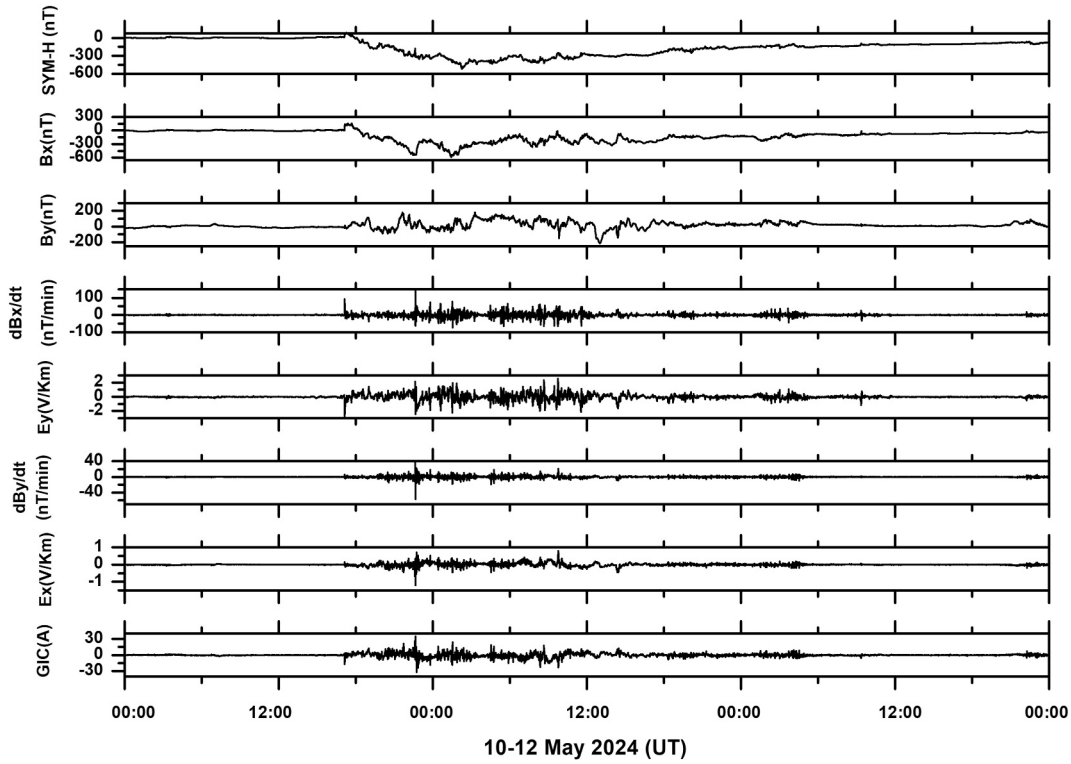

Figure 10. Analysis of the effects of geomagnetic disturbance at Manzhouli substation. The panels, from top to bottom, show the SYM-H index, the north and east component of the observed geomagnetic field at OMZLN (B_x, B_y), dB_x/dt, the calculated east component of the geoelectric field (E_y), dB_y/dt, the calculated north component of the geoelectric field (E_x), and the calculated geomagnetically induced current at the Manzhouli substation during May 10–12,2024.

A strong geoelectric field emerging during the SSC may trigger an abrupt power grid accident. If the geoelectric field remains high for a long time, the resulting GICs may cause transformer heating, mechanical vibration, and reactive power loss. Potential disconnection from service is possible, which may in turn initiate a cascade of failure within the power grid. Close monitoring of geomagnetic storms exhibiting such characteristics is necessary and proactive mitigation tactics should be considered.

To better understand the distribution of GICs across the power grid and identify the most affected substations, the maximum GIC values at part of the substations flowing through the common ground during this storm are plotted in Figure 11. It is observed that, due to the corner effect (Boteler et al., 1994), the maximum GICs at the Arxan, Hailuto, Muchang, and Taiben substations located at the end of the power grid topology are larger than those of nearby transformers. Additionally, the maximum GICs at the Boketu, Baolongshan, Jingouliang, and Wudan substations located at corners are also larger. When considering extremely hazardous accidents such as geomagnetic storms, characterized by "low probability but high risk", the power grid defense plan should prioritize addressing the GIC effect in low conductivity areas, line corners, end of the power grid topology, and boundary nodes. The capability to accurately simulate GICs at substations lacking direct monitoring devices is particularly valuable for comprehensive power grid risk assessment and for prioritizing the installation of GIC monitoring equipment at the most vulnerable substations identified through modeling.

As the voltage level increases, there is a notable reduction in the resistance per unit length of the conductor. Specifically, for a 1,000 kV conductor, its resistance per unit length is less than half that of a 500 kV conductor. Furthermore, when raising the voltage level both the transmission distance and scale increase, leading to a corresponding GIC magnitude enhancement within the grid. The simulated GICs flowing through the common grounding points of Baolongshan(with the highest GIC level at 220 kV), Fengtun (with the highest GIC level at 500 kV), and Tianjin South (with the highest GIC level at 1,000 kV) substations are depicted in Figure 12. The largest GIC variations at Baolongshan, Fengtun, and Tianjin South substations are 48.8 A, −76.7 A, and 168.5 A, respectively.

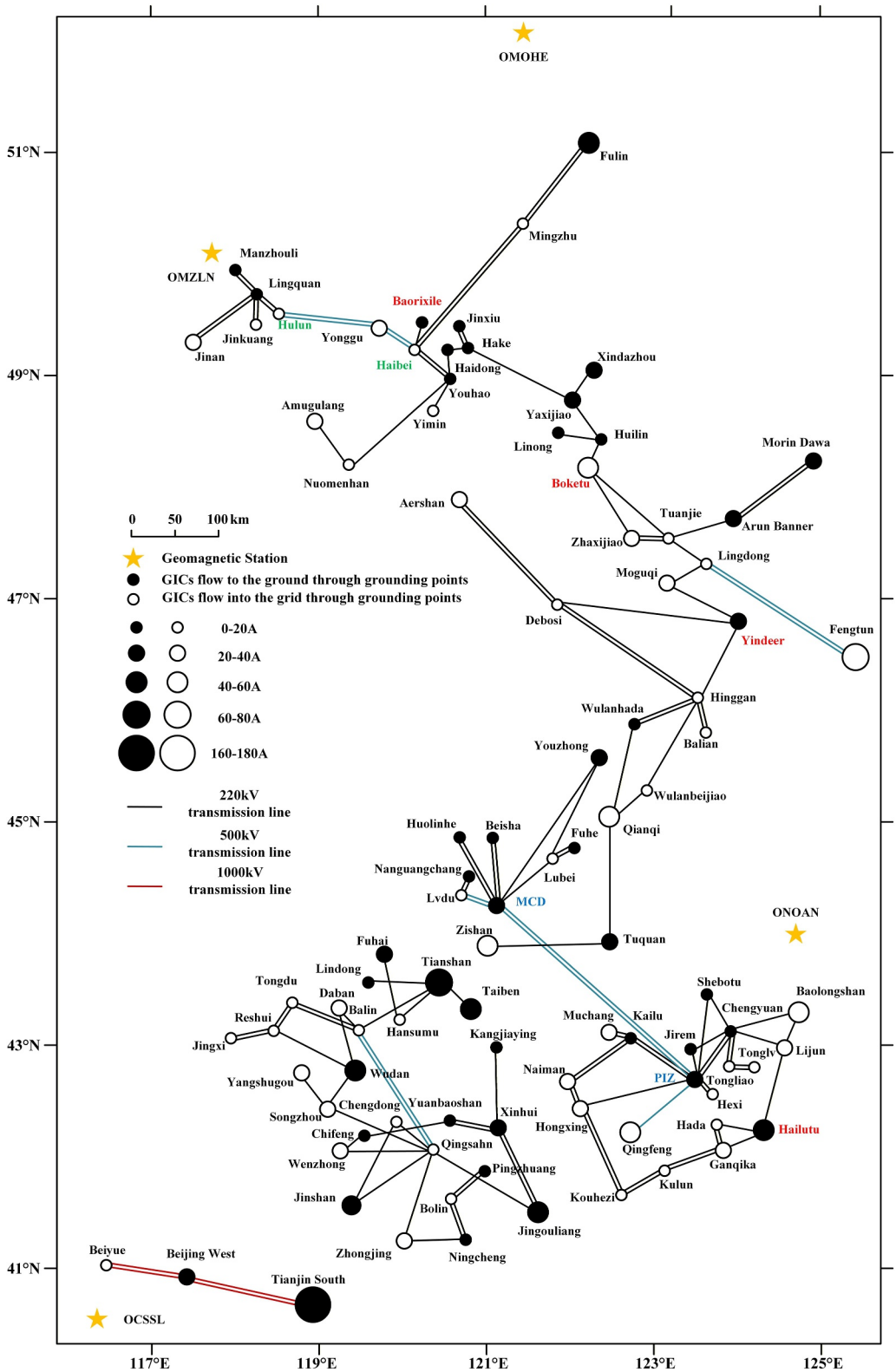

Figure 11. Spatial distribution of the maximum geomagnetically induced currents (GICs) at part of the substations in the Eastern Inner Mongolia Power Grid during the May 2024 storm. The size of the circle is scaled with the magnitude of the GICs. Hollow and filled circles represent the GICs that flow into the grid and into the Earth, respectively. The yellow stars denote the geomagnetic stations. The MCD Substation and PIZ Substation are marked in blue font.

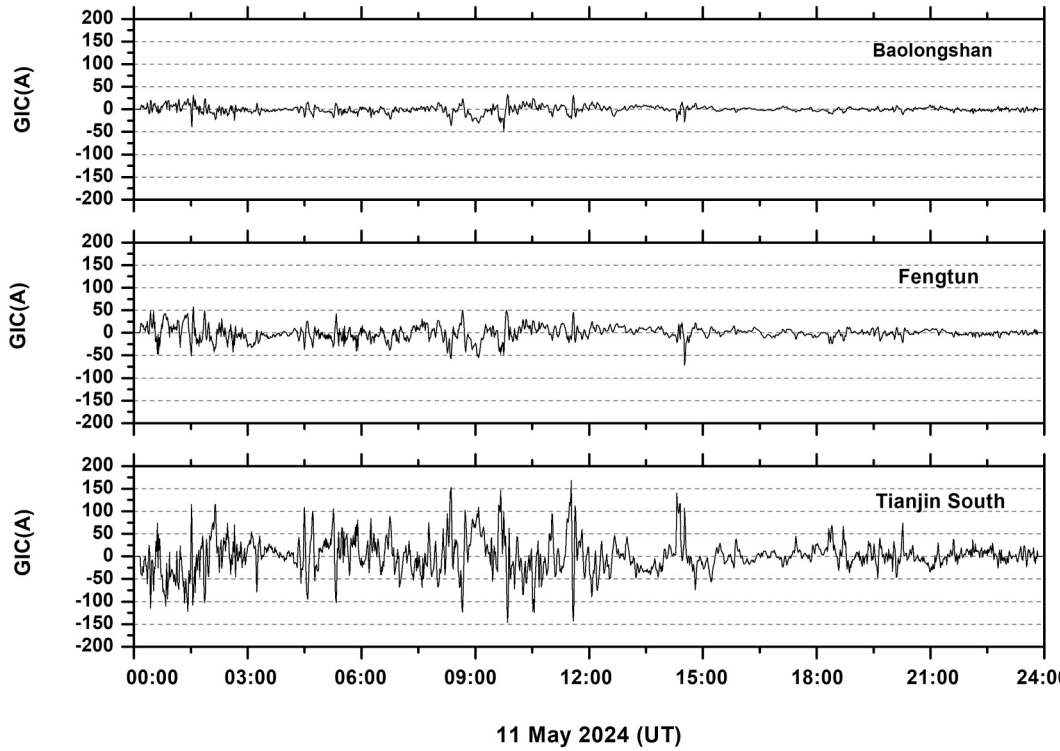

Figure 12. Geomagnetically induced current simulations at Baolongshan (220 kV), Fentun (500 kV) and Tianjin South (1,000 kV) substations.

The impact of geomagnetic storms on power grid components is primarily considered in relation to transformers. The increase and distortion of excitation current caused by DC-biased magnetization in transformers lead to higher reactive power loss (Dong et al., 2001; Molinski, 2002). Since geomagnetic storms occur synchronously on a global scale, GICs can cause hundreds of transformers across the power grid to simultaneously experience magnetic saturation, resulting in reactive power deficiency throughout the system. This can induce reactive power fluctuations and voltage drops. Moreover, the distorted excitation current contains a large number of harmonic components, which may trigger maloperation of various protective relays (Marti et al., 2014; Walling & Khan, 1991). Among the most affected are those reactive power compensation devices such as shunt capacitor banks and static var compensators. If these devices are forced out of service during period of reactive power deficiency, voltage collapse (Boteler et al., 1998; Kappenman, 2010) and even large-scale blackout in the power grid can happen.

Among all transformers, the GIC of the 1,000 kV voltage level Tianjin South substation was the highest. Its transformer excitation current was analyzed by computing the excitation current curve under DC bias conditions. Given that the maximum GIC through the transformer neutral point was 168.5 A, the maximum GIC flowing through its single-phase winding was approximately 56.2 A. The excitation current over a 20 ms power-frequency cycle, under the condition with GIC of 56.2 A and without GIC, was calculated using the field-circuit coupled three-dimensional finite element method (Li et al., 2020), as shown in the left panel of Figure 13. During the saturated half-cycle, the alternating magnetic flux was in the same direction as the DC flux induced by the GIC. The combined magnetic flux exceeded the knee point of the core's B–H curve, which drove the core into a saturation status and significantly reduced its magnetic permeability. This resulted in a sharp excitation current peak (Liu & Liu, 1993) observed at 5 ms (a quarter cycle). In contrast, during the unsaturated half-cycle, the alternating magnetic flux opposed the DC flux. The net flux was thereby reduced compared to the GIC-free case, hence the core was unsaturated and maintained at high magnetic permeability. Consequently, the excitation current dropped sharply to a very low level. As illustrated in the left panel of Figure 13, when a 56.2 A GIC is applied, the excitation current peak remarkably increases from 16.2 to 439.4 A. A discrete Fourier transform analysis was then applied to the excitation current. The right panel of Figure 13 displays the harmonic amplitudes under GIC and non-GIC conditions. Since the distortion is primarily concentrated below the 10th harmonic and

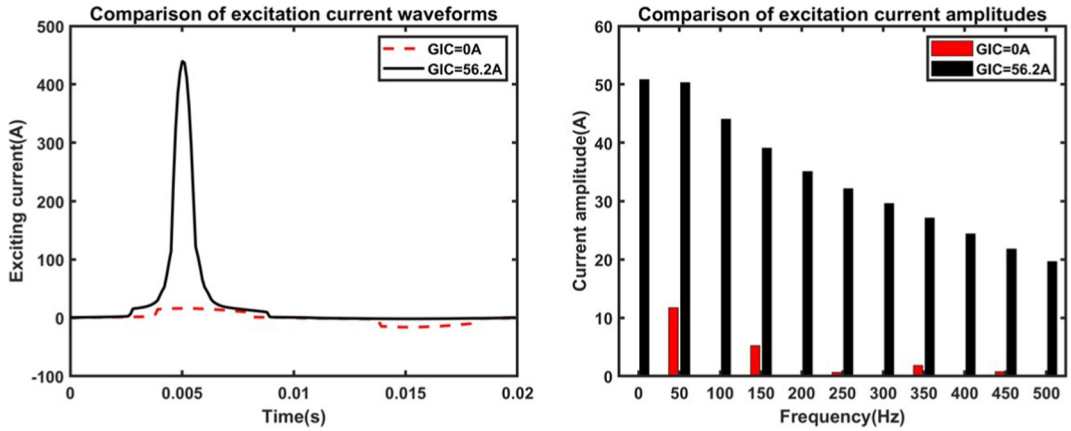

Figure 13. Excitation current waveform and its harmonic spectrum of the transformer at Tianjin South substation when the geomagnetically induced current reached its maximum.

higher-order harmonics exhibit limited sensitivity to the DC-biased magnetization current, only harmonic components below the 10th order are displayed in the figure. It is evident that the presence of GIC increases the amplitude of all harmonic components, with even-order harmonics showing more pronounced enhancement. Moreover, harmonic amplitude generally decreases with increasing harmonic order.

The total harmonic distortion (THD) was employed to characterize the degree of current distortion under DC-biased conditions. The THD is defined as the ratio of the root mean square (RMS) value of the higher-order harmonic components to the fundamental component, expressed by:

$$\mathrm{THD} = \sqrt{I_2^2 + I_2^3 + I_2^4}/I_1 \tag{9}$$

When the neutral point current of the transformer at the Tianjin South substation reached a maximum value of 168.5 A, the THD was as high as 205.85%, indicating a high level of distortion. While this level of THD can lead to transformer heating, vibration, and reactive power consumption, it does not necessarily result in immediate system failure. However, IEEE Standard C57.110–2018 recommends that THD should not exceed 5% under normal operating conditions. Total harmonic distortion values exceeding 200% represent extreme conditions that significantly increase the risk of protection relay misoperation, accelerated insulation aging, and cumulative damage to transformer cores. During the Mother's Day storm, despite this high THD value, no catastrophic failures occurred in the Eastern Inner Mongolia Power Grid, likely due to the relatively short duration of peak GIC activity and the inherent design margins in modern UHV transformers.

3.3. Comparison With Historical Major Geomagnetic Storms

We compared the Mother's Day storm to two severe historical geomagnetic storms: (a) the well-known event from March 13 to 15, 1,989 (Dst = −589 nT) that led to a power outage in Quebec, Canada, and (b) the extreme geomagnetic storm from November 9 to 10, 2004 (Dst = −263 nT), during which the neutral-point monitored GIC of a 500 kV transformer at the Guangzhou Ling'ao Nuclear Power station reached 75.5 A (Liu et al., 2009). By substituting the geomagnetic data provided by the Beijing Geomagnetic Station affiliated with the Institute of Geophysics, China Earthquake Administration for the periods of March 13–15, 1,989 and November 9–10, 2004 into the Eastern Inner Mongolia Power Grid model, we have figured out that the maximum induced geoelectric field strength of the 2024 geomagnetic storm event is 1.69 V/km, which exceeds the 2004 event by 88% (0.9 V/km) and is within 0.6% of the intensity observed during the 1,989 storm (1.7 V/km). These results indicate that the 2024 storm's impact on the Eastern Inner Mongolia Power Grid was nearly identical to the extreme 1,989 storm and more severe than the 2004 event. Table 4 presents the simulated maximum GICs at selected substations representing different voltage levels and geographic locations within the Eastern Inner Mongolia Power Grid. The selection includes: (a) the three substations (Baolongshan, Fengtun, and Tianjin South) discussed previously as having the highest GICs at each voltage level, (b) substations located at grid corners or terminals where the

Table 4
The Simulated Maximum Geomagnetically Induced Currents at Part of the Eastern Inner Mongolia Power Grid Substations During the 1,989, 2004 and 2024 Storm

Voltage class	Substation	1989 GIC (A)	2004 GIC (A)	2024 GIC (A)
1000 kV	Tianjin South	185.3	63.4	168.5
	Beijing West	43.9	40.8	39.6
	Beiyue	10.8	5.7	12.7
500 kV	Fengtun	51.9	21.5	76.7
	Lvdu	12.6	10.5	15.5
	Qingfeng	55.9	29.3	52.5
220 kV	Baolong Mountain	108.3	57.3	48.8
	Fulin	60.1	33.4	57.3
	Tuquan	32.7	17.5	26.4
	Tianshan	69.8	53.6	78.8
	Jingouliang	60.5	18.2	55.9
	Yindeer	71.1	37.7	39.6

'corner effect' amplifies GIC magnitude, and (c) substations distributed across different latitudes to illustrate spatial variability. The 220 and 500 kV substations in Table 4 meet both the second and third selection criteria. This selection provides a representative overview of GIC distribution patterns across the network.

Note that during the geomagnetic storms in 1989 and 2004, the geomagnetic field measurement was only available from the Beijing geomagnetic station. Using data from a single geomagnetic station to represent the entire power grid fails to account for the spatial variability of magnetosphere–ionosphere current systems. This simplification may introduce errors in the GIC estimation and hence in evaluating the storm's actual impact. In contrast, for the May 2024 storm, an interpolation method based on equivalent ionospheric current inversion was employed to reconstruct the geomagnetic field input at a specified location, which was more accurate for regional estimation. If the geoelectric field was computed using only the Beijing geomagnetic station data for the 2024 storm, the maximum induced geoelectric field would reach 2.14 V/km, more than that calculated using the SECS method. Analogously, the actual impact of the 1,989 and 2004 storms would have been even less severe than what was previously assessed. On the other hand, the GIC simulations for these three geomagnetic storms were conducted based on the current configuration of the Eastern Inner Mongolia Power Grid. In brief, the result only represents a hypothetical comparison and is not granularity-consistent, nevertheless it indicates the potential GIC levels of similar intense storms for a particular power grid configuration as much as possible.

Although the simulated impact of the 2024 storm on the Eastern Inner Mongolia Power Grid was comparable to that of the 1,989 storm, it did not cause any major grid incident as the latter led to a blackout in the Québec power grid. In fact, geomagnetic storms are only one of the potential triggers to cause power grid failure, including equipment manufacturing defects, aging, load conditions, inadequate maintenance, human operational errors, suboptimal grid design and planning, and improper dispatch and operation strategies, to name a few.

4. Discussion

The CMP Geomagnetic Observatory Network spans nearly the entire mainland China with outstanding capabilities and advantages. The network provides geomagnetic field data, which support the GIC related research in measurement, modeling, forecasting, and hazard assessment. Using the geomagnetic monitoring instruments of CMP, we surveyed the geomagnetic disturbance over China and the GICs in the Eastern Inner Mongolia Power Grid during the Mother's Day storm. The simulated GICs at two 500 kV substations in the Eastern Inner Mongolia Power Grid agreed well with the measurements made by the on-site monitoring devices in both the variation trend and the peak amplitude. The results confirm the satisfactory level of accuracy of the GIC modeling proposed in this study. It is reliable to serve as an early warning/forecast tool and provides a basis for risk assessment when an extreme space weather event happens. Although the overall RMS error between the measured and simulated values was

approximately 1 A, the comparison yielded valuable insights for validating and refining the relevant disaster prediction models, and thereby enabling more precise guidance for future extreme events. Unfortunately, no valid GIC data were recorded during the peak of the storm on May 11 due to equipment failure. It highlights the importance of preventive maintenance and inspection of the GIC monitoring systems to prevent data loss that may compromise the subsequent grid dispatch and control strategies. The performance of the GIC monitoring devices and the accuracy of the CMP geomagnetic field observation were commendable during this extreme geomagnetic storm, implying that real-time monitoring of the space weather effect on the power grid over China and timely operational responses are possible.

There were records at mid- and low-latitude regions during this magnetic storm. For example, the observed GIC of the transformer neutral at the 400 kV Laguna Verde, Veracruz (LAV, 19.72°N, 96.41°W) station of the Mexican power grid (R. Caraballo et al., 2025) peaked at ∼30 A (Caraballo et al., 2025). Interestingly, the GIC measured at the 330 kV main power line of the Kondopoga substation located in the subauroral region (geographic: 62.2°N, 34.3°E) triggered a peak of ∼40 A (Hajra et al., 2024) while the GIC through one of the windings of the lower latitude Tianjin South substation peaked at a larger value of 56.2 A. That was due to the significantly higher voltage level of Tianjin South substation and its location at the transmission line terminus. As shown in Figure 11, voltage level has a greater influence on the GIC distribution than latitude does. Geomagnetically induced current magnitude tends to be higher at substations with higher voltage level. Tianjin South substation, operating at a voltage level of 1,000 kV, exhibited the highest GIC in the grid that was a three-phase total maximum of 168.5 A. Fortunately, GICs typically pose extreme risks above the threshold of 200 A and the power grid has some inherent resilience against GICs in the subsequent stages. As a result, such a high GIC level at Tianjin South substation did not cause any damage. The simulated maximum GIC at the neutral of the 500 kV Fengtun substation reached 76.7 A. It was comparable to the 75.5 A observed at the neutral of the 500 kV Ling Ao Nuclear Power Station (22.6°N, 114.6°E) in Guangdong Province on 10 November 2004, where the transformer noise anomalies and vibration incidents were reported (Liu et al., 2009). Although the Mother's Day geomagnetic storm did not cause catastrophic damage to the Eastern Inner Mongolia grid, the cumulative effects of extreme geomagnetic disturbances remain uncertain. Modern Chinese transmission lines use large cross-section conductors (e.g., $4 \times 630\ mm^2$ at 500 kV, $6 \times 400\ mm^2$ at 750 kV, and $8 \times 500\ mm^2$ at 1,000 kV), which reduce resistance and increase GIC susceptibility. The accelerated development of ultra-high-voltage (UHV) networks and increasing interconnection among grids are expected to elevate operational uncertainties and GIC levels and thereby the disaster risks associated with extreme space weather are heightened. These findings emphasize the urgent need for effective forecasting techniques and the implementation of robust mitigation strategies against geomagnetic hazard.

As part of the global effort to understand the space weather effects, the CMP monitoring network provides observations that help clarify the regional characteristics of the space environment over China. The project promotes important innovative scientific achievements and has already operated efficiently for more than 10 yrs. The massive high-quality monitoring data effectively support both the frontier scientific research in the subject of space physics and the operational space weather forecast in China.

5. Summary

In this study, we analyzed the geomagnetic disturbances over China using the data from a total of 23 CMP geomagnetic stations during the super storm of May 10–12, 2024. The observations demonstrated a clear SSC at 17:07 UT on 10 May 2024 and a strong, long-lasting storm main phase before the disturbance gradually returned to the quiet level. During the main phase, the recorded minimum B_h and absolute peak value of dB_h/dt in the East Mongolia Power Grid service area were −720 nT and 60 nT/min, respectively. The results also showed that geomagnetic disturbances in this area were stronger than those in other regions of China.

Conventional GIC measurement techniques rely on neutral-point. However, the GIC monitoring devices in two 500 kV substations of the Eastern Inner Mongolia Power Grid were installed on the high-voltage transformer incoming lines. This configuration ensures electrical isolation between the GIC monitoring system and the high-voltage, high-current infrastructure, and thereby overcomes the insulation limitation that is commonly encountered in neutral-point GIC measurements. Comparison of the simulated GICs to the measurement indicates that the simulation model is capable of correctly predicting the GICs. Analysis revealed a high correlation between the measured and calculated GIC data, which further validated the monitoring device's accuracy. The GIC monitoring devices installed on the transformer high-voltage lines provide reliable measurements and support long-term

monitoring. This configuration enables accurate real-time tracking of GICs during geomagnetic storms, helping secure stable operation of the power grid.

During the May 2024 super storm, the time derivative of the geomagnetic field at the Manzhouli substation in the Eastern Inner Mongolia Power Grid showed a sharp fluctuation at the SSC, which coincided with the maximum induced geoelectric field. Subsequently, the maximum GIC was recorded in the main phase. Geomagnetic storms characterized by high-magnitude geoelectric fields in the initial phase particularly tend to trigger progressive grid disturbances and cumulative effects, which are difficult to prevent.

Further analysis of the spatial distribution of the estimated maximum GICs during the storm revealed that the most severely affected areas were located along the edges of the power grid, particularly line corners and terminals. Baolongshan (220 kV), Fengtun (500 kV), and Tianjin South (1,000 kV) substations recorded the highest GIC amplitudes at their respective voltage levels, indicating that these substations are likely to be at high risk during future extreme geomagnetic events. Accordingly, it is recommended that for future grid planning, priority should be given to: (a) replacing transformers at these critical substations with high GIC-tolerant modules and (b) installing GIC blocking or mitigation devices at other substations that exhibit significant neutral point GIC levels. Such proactive measures would substantially enhance the resilience of the power grid against extreme geomagnetic storms.

Appendix A

Figure A1 presents the amplitude variation of the H component (B_h) at the 23 CMP stations during 9–12 May 2024. All stations show responses to the geomagnetic storm, with the stations located near the East Inner Mongolia Power Grid exhibited relatively stronger geomagnetic disturbances compared to other stations.

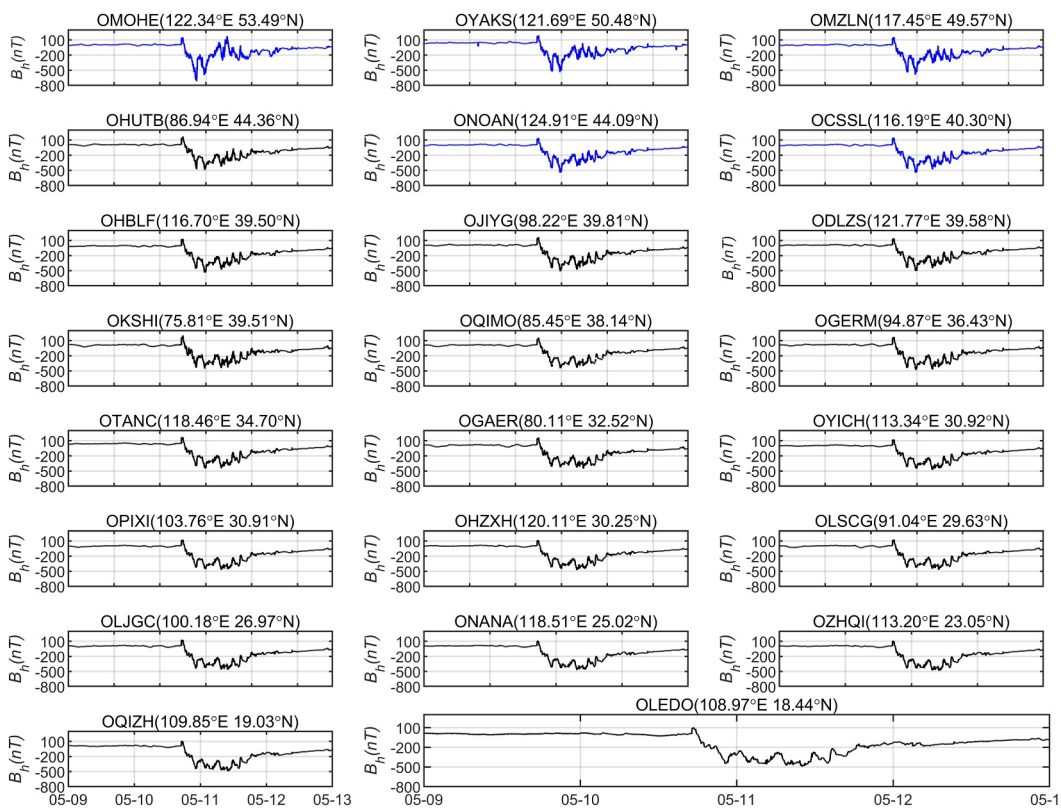

Figure A1. The amplitude variation of the H component (B_h) at the 23 Chinese Meridian Project stations during 9–12 May 2024. The blue lines show the B_h observed at the geomagnetic stations located near the East Inner Mongolia Power Grid while the black lines show the B_h of other stations.

Figure A2 presents the evolution of the magnetic field map in Chinese region. When the geomagnetic field is quiet, the H component has insignificant variation. During the SSC, the geomagnetic field showed upward trend in the H component vector. During the main phase of the storm, the geomagnetic field accompanied by downward variation in vector direction.

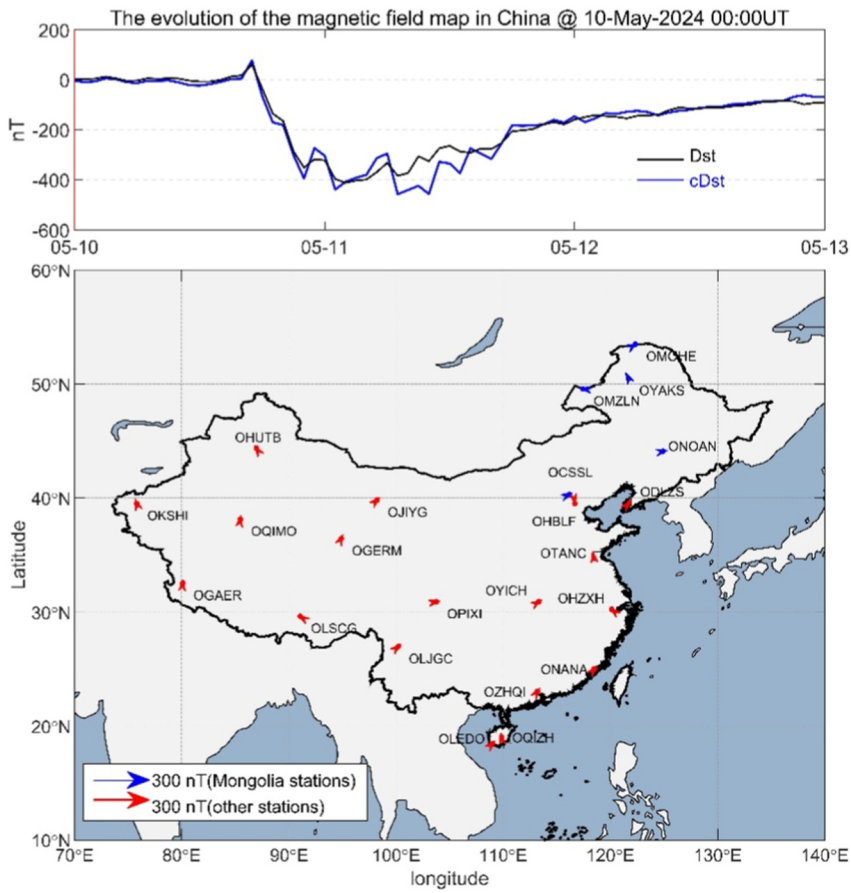

Figure A2. The evolution of the magnetic field map in Chinese region.

Figure A3 presents the time derivative of the horizontal component of the geomagnetic perturbations (dB_H/dt) from the 23 CMP stations during May 9–12, 2024. The stations located near the East Inner Mongolia Power Grid exhibited relatively stronger dB_H/dt compared to other stations.

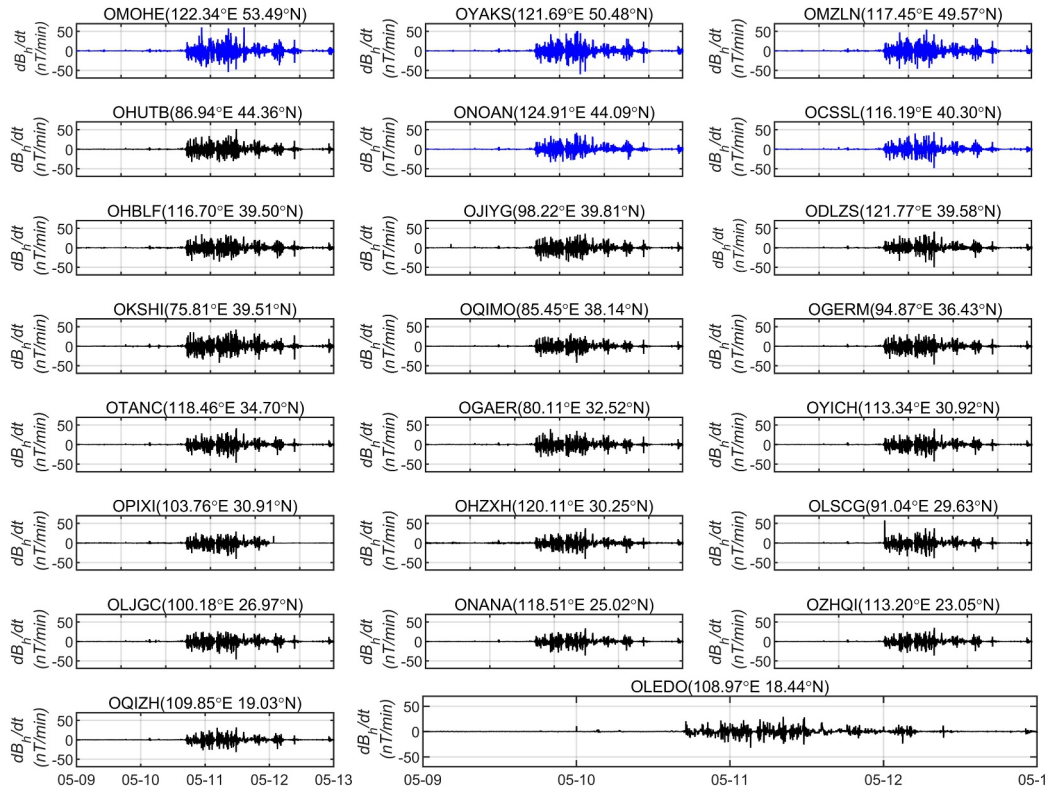

Figure A3. The time derivative of the horizontal component of the geomagnetic perturbations (dB_H/dt) from the 23 Chinese Meridian Project stations during May 9–12, 2024. The blue lines represent the stations located near the East Inner Mongolia Power Grid while the black lines represent the other stations.

Conflict of Interest

The authors declare no conflicts of interest relevant to this study.

Data Availability Statement

The Dst index, SYM-H index and IQDs are from are from World Data Center for Geomagnetism, Kyoto (World Data Center for Geomagnetism, 2024). The cDst index data are from (Li et al., 2025). The geomagnetic field data during May 10–12, 2024 of the 23 geomagnetic stations in China can be obtained from the Chinese Meridional Project (Chinese Meridional Project, 2024). The geomagnetic data during March 13–15, 1989 and November 9–10, 2004 are provided by the Institute of Geophysics, China Earthquake Administration (China Earthquake Administration, 2024).

Acknowledgments
This work is supported by the National Key R&D Program of China (Grant 2024YFC2206902, Grant 2022YFF0504400, Grant 2025YFE0202500), the Strategic Priority Research Program of the Chinese Academy of Sciences (Grant XDB0560000), the General Program of National Natural Science Foundation of China (Grant 52177081, 42374198, 42188101, 42504172, 42574233), the project of Civil Aerospace "14th Five Year Plan" Preliminary Research in Space Science (Grant D010202, D010301), the China-Brazil Joint Laboratory for Space Weather (Grant 119GJHZ2024027MI), the Chinese Sponsored Postdoctoral Fellowship Program (Grant GZC20232695). We acknowledge the use of the ground-based data from the CMP and the GIC data from the Eastern Inner Mongolia Power Grid.

References

Aa, E., Zhang, S.-R., Lei, J., Huang, F., Erickson, P. J., Coster, A. J., et al. (2024). Significant midlatitude plasma density peaks and dual-hemisphere SED during the 10-11 May 2024 super geomagnetic storm. *Journal of Geophysical Research: Space Physics*, *129*(11), e2024JA033360. https://doi.org/10.1029/2024JA033360

Amm, O. (1997). Ionospheric elementary current systems in spherical coordinates and their application. *Journal of Geomagnetism and Geoelectricity*, *49*(7), 947–955. https://doi.org/10.5636/jgg.49.947

Araki, T. (1994). A physical model of the geomagnetic sudden commencement. *Geophys. Monograph-American Geophys. Union*, *81*, 183–200. https://doi.org/10.1029/GM081p0183

Beggan, C. D. (2015). Sensitivity of geomagnetically induced currents to varying auroral electrojet and conductivity models. *Earth Planets and Space*, *67*(24), 1–12. https://doi.org/10.1186/s40623-014-0168-9

Bolduc, L., Gaudreau, A., & Dutil, A. (2000). Saturation time of transformers under dc excitation. *Electric Power Systems Research*, *56*(2), 95–102. https://doi.org/10.1016/S0378-7796(00)00087-0

Boteler, D. (2000). Geomagnetic effects on the pipe-to-soil potentials of a continental pipeline. *Advances in Space Research*, *26*(1), 15–20. https://doi.org/10.1016/S0273-1177(99)01020-0

Boteler, D. (2014). Methodology for simulation of geomagnetically induced currents in power systems. *Journal of Space Weather and Space Climate*, *4*, A21. https://doi.org/10.1051/swsc/2014018

Boteler, D. H., & Bradley, E. (2016). On the interaction of power transformers and geomagnetically induced currents. *IEEE Transactions on Power Delivery*, *31*(5), 2188–2195. https://doi.org/10.1109/TPWRD.2016.2576400

Boteler, D. H., Bui-Van, Q., & Lemay, J. (1994). Directional sensitivity to geomagnetically induced currents of the hydro-quebec 735 kv power system. *IEEE Transactions on Power Delivery*, *9*(4), 1963–1971. https://doi.org/10.1109/61.329528

Boteler, D. H., & Pirjola, R. J. (2017). Modeling geomagnetically induced currents. *Space Weather*, *15*(1), 258–276. https://doi.org/10.1002/2016SW001499

Boteler, D. H., Pirjola, R. J., & Nevanlinna, H. (1998). The effects of geomagnetic disturbances on electrical systems at the Earth's surface. *Advances in Space Research*, *22*(1), 17–27. https://doi.org/10.1016/S0273-1177(97)01096-X

Cagniard, L. (1953). Basic theory of the magneto-telluric method of geophysical prospecting. *Geophysics*, *18*(3), 605–635. https://doi.org/10.1190/1.1437915

Caraballo, R., González-Esparza, J. A., Pacheco, C. R., Corona-Romero, P., Arzate-Flores, J. A., & Castellanos Velazco, C. I. (2025). The impact of geomagnetically induced currents (GIC) on the Mexican power grid: Numerical modeling and observations from the 10 May, 2024, geomagnetic storm. *Geophysical Research Letters*, *52*(4), e2024GL112749. https://doi.org/10.1029/2024GL112749

Chen, Y. H., Ercha, A. A., Yuan, T. J., Zhang, S. h. R., Shen, H., Yue, X., et al. (2025). The extreme depletion of ionospheric electron density and its hemispheric asymmetry during the May 2024 storm. *National Science Review*, *12*(10), nwaf307. https://doi.org/10.1093/nsr/nwaf307

China Earthquake Administration. (2024). The geomagnetic data during March 13-15, 1989 and November 9-10, 2004. Retrieved from http://data.earthquake.cn

Chinese Meridional Project. (2024). The geomagnetic field data during May 10-12, 2024 of the 23 geomagnetic stations in China. Retrieved from https://data.meridianproject.ac.cn

Dong, X., Liu, Y., & Kappenman, J. G. (2001). Comparative analysis of exciting current harmonics and reactive power consumption from GIC saturated transformers. *In 2001 IEEE power engineering society winter meeting. Conference proceedings (Cat. No. 01CH37194)*, (Vol. 1, pp. 318–322). IEEE. https://doi.org/10.1109/PESW.2001.917055

Hajra, R., Tsurutani, B. T., Lakhina, G. S., Lu, Q., & Du, A. (2024). Interplanetary causes and impacts of the 2024 may superstorm on the geosphere: An overview. *The Astrophysical Journal*, *974*(2), 264–275. https://doi.org/10.3847/1538-4357/ad7462

Hayakawa, H., Yusuke, E., Alexander, M., et al. (2024). The solar and geomagnetic storms in May 2024: A flash data report. *The Astrophysical Journal*, *979*(1), 264–275. https://doi.org/10.3847/1538-4357/ad9335

Horton, R., Boteler, D., Overbye, T. J., Pirjola, R., & Dugan, R. C. (2015). A test case for the calculation of geomagnetically induced currents. *IEEE Transactions on Power Delivery*, *27*(4), 2368–2373. https://doi.org/10.1109/TPWRD.2012.2206407

Jonas, S., & McCarron, E. D. (2015). Recent U.S. policy developments addressing the effects of geomagnetically induced currents. *Space Weather*, *13*(11), 730–733. https://doi.org/10.1002/2015SW001310

Kappenman, J. (2010). Geomagnetic storms and their impacts on the US power grid (Meta-R-319). *ORNLFERC Report*. Weblink http://www.ornl.gov/sci/ees/etsd/pes/ferc_emp_gic.shtml

Kwak, Y. S., Kim, J. H., Kim, S., Miyashita, Y., Yang, T., Park, S. H., et al. (2024). Observational overview of the May 2024 G5-Level geomagnetic storm: From solar eruptions to terrestrial consequences. *Journal of Astronomy and Space Sciences*, *41*(3), 171–194. https://doi.org/10.5140/JASS.2024.41.3.171

Lawrence, E., Beggan, C. D., Richardson, G. S., Reay, S., Thompson, V., Clarke, E., et al. (2025). The geomagnetic and geoelectric response to the May 2024 geomagnetic storm in the United Kingdom. *Frontiers in Astronomy and Space Sciences*, *12*, 1550923. https://doi.org/10.3389/fspas.2025.1550923

Li, B., Wang, Z., Li, M., & Guo, S. (2020). Analysis of the DC bias effects on the UHV autotransformer with rated load based on a reduced-scale model experiment. *Applied Sciences*, *10*(4), 1529. https://doi.org/10.3390/app10041529

Li, H., & Liu, Z. (2023). A dataset of Dst Indexes in China (2010–2022). *China Scientific Data*, *4*, 329–335. https://doi.org/10.11922/11-6035.csd.2023.0079.zh

Li, H., Liu, Z., & Wang, J. (2025). The Dst index in China (cDst index) on 10-12 May 2024 (Version 1) [Dataset]. *Science Data Bank*. https://doi.org/10.57760/sciencedb.27906

Liu, C. M., Liu, L. G., & Pirjola, R. (2009). Geomagnetically induced currents in the high-voltage power grid in China. *IEEE Transactions on Power Delivery*, *24*(4), 2368–2374. https://doi.org/10.1109/TPWRD.2009.2028490

Liu, L., Ge, X., Zong, W., Zhou, Y., & Liu, M. (2016). Analysisof themonitoring data of geomagneticstorm interference inthe electrification system of a high-speed railway. *Space Weather*, *14*(10), 754–763. https://doi.org/10.1002/2016SW001411

Liu, S., & Liu, Y. (1993). Fem analysis of dc saturation to assess transformer susceptibility to geomagnetically induced currents. Power Delivery. *IEEE Transactions on*, *8*(3), 1367–1376. https://doi.org/10.1109/61.252663

Liu, W., Liu, G. X., & Han, J. T. (2008). Research on Xilamulun fault east extension based on evidence of magnetotelluric sounding data. *Global Geology*, *27*(1), 89–94. https://lib.cqvip.com/Qikan/Article/Detail?id=26819966

Marti, L., Yiu, C., Rezaei-Zare, A., & Boteler, D. (2014). Simulation of geomagnetically induced currents with piecewise layered-earth models. *IEEE Transactions on Power Delivery*, *29*(4), 1886–1893. https://doi.org/10.1109/TPWRD.2014.2317851

Matsushita, S. (1962). On geomagnetic sudden commencements, sudden impulses, and storm durations. *Journal of Geophysical Research*, *67*(10), 3753–3777. https://doi.org/10.1029/jz067i010p03753

Molinski, T. S. (2002). Why utilities respect geomagnetically induced currents. *Journal of Atmospheric and Solar-Terrestrial Physics*, *64*(16), 1765–1778. https://doi.org/10.1016/S1364-6826(02)00126-8

Piersanti, M., Oliveira, D. M., D'Angelo, G., Diego, P., Napoletano, G., & Zesta, E. (2025). On the geoelectric field response to the SSC of the May 2024 super storm over Europe. *Space Weather*, *23*, e2024SW004191. https://doi.org/10.1029/2024SW004191

Pirjola, R. (2002). Review on the calculation of surface electric and magnetic fields and of geomagnetically induced currents in ground-based technological systems. *Surveys in Geophysics*, *23*(1), 71–90. https://doi.org/10.1023/A:1014816009303

Pulkkinen, A., Bernabeu, E., Thomson, A., Viljanen, A., Pirjola, R., Boteler, D., et al. (2017). Geomagnetically induced currents: Science, engineering, and applications readiness. *Space Weather*, *15*(7), 819–970. https://doi.org/10.1002/2016SW001501

Spogli, L., Alberti, T., Bagiacchi, P., Cafarella, L., Cesaroni, C., Cianchini, G., et al. (2024). The effects of the May 2024 Mother's Day superstorm over the mediterranean sector: From data to public communication. *Annals of Geophysics*, *67*(2), PA218. https://doi.org/10.4401/ag-9117

Viljanen, A., Pulkkinen, A., Amm, O., Pirjola, R., & Korja, T., & BEAR Working Group. (2004). Fast computation of the geoelectric field using the method of elementary current systems and planar Earth models. *Annales Geophysicae*, *22*(1), 101–113. https://doi.org/10.5194/angeo-22-101-2004

Waghule, B., & Knipp, D. J. (2024). *Ionospheric response during the 10-12 May 2024 geomagnetic storm and its connection to GICs. 2025 United States National Committee of URSI National Radio Science Meeting* (pp. 362–363). USNC-URSI NRSM). https://doi.org/10.23919/USNC-URSINRSM66067.2025.10973159

Walling, R. A., & Khan, A. N. (1991). Characteristics of transformer exciting-current during geomagnetic disturbances. *IEEE Transactions on Power Delivery*, *6*(4), 1707–1714. https://doi.org/10.1109/61.97710

Wang, C. (2010). New chains of space weather monitoring stations in China. *Space Weather*, *8*, S08001. https://doi.org/10.1029/2010SW000603

Wang, C., Xu, J., Chen, Z., Li, H., Feng, X., Huang, Z., & Wang, J. (2024). China's ground-based space environment monitoring network—Chinese Meridian Project (CMP). *Space Weather*, *22*, e2024SW003972. https://doi.org/10.1029/2024SW00397

Wang, X., Aa, E., Chen, Y. H., Zhang, J. J., Zhu, Y., Cai, L., et al. (2025). Midlatitude neutral wind response during the mother's day super-intense geomagnetic storm in 2024 using observations from the Chinese Meridian Project. *Journal of Geophysical Research: Space Physics*, *130*(4), e2024JA033574. https://doi.org/10.1029/2024JA033574

World Data Center for Geomagnetism. (2024). The Dst index, SYM-H index and International Quiet Days. Retrieved from https://wdc.kugi.kyoto-u.ac.jp/index.html

Zhang, J. J., Yu, Y. Q., Chen, W. Q., Wang, C., Liu, Y. D., Liu, C. M., & Liu, L. G. (2022). Simulation of geomagnetically induced currents in a low-latitude 500 kV power network during a solar superstorm. *Space Weather*, *20*(4), e2021SW003005. https://doi.org/10.1029/2021SW003005

Zhang, J. J., Yu, Y. Q., Wang, C., Du, D., Wei, D., & Liu, L. G. (2020). Measurements and simulations of the geomagnetically induced currents in low-latitude power networks during geomagnetic storms. *Space Weather*, *18*(8), e2020SW002549. https://doi.org/10.1029/2020SW002549